# Gold Helix Photonic Metamaterial as Broadband Circular Polarizer

Justyna K. Gansel,[1]* Michael Thiel,[1] Michael S. Rill,[1] Manuel Decker,[1] Klaus Bade,[2] Volker Saile,[2] Georg von Freymann,[1,3] Stefan Linden,[1,3] Martin Wegener[1,3]

We investigated propagation of light through a uniaxial photonic metamaterial composed of three-dimensional gold helices arranged on a two-dimensional square lattice. These nanostructures are fabricated via an approach based on direct laser writing into a positive-tone photoresist followed by electrochemical deposition of gold. For propagation of light along the helix axis, the structure blocks the circular polarization with the same handedness as the helices, whereas it transmits the other, for a frequency range exceeding one octave. The structure is scalable to other frequency ranges and can be used as a compact broadband circular polarizer.

Metamaterial research has largely been stimulated by proposals and demonstrations of negative phase velocities (1–3), "perfect lenses" (4), or invisibility cloaking (5–7). Strong chirality has brought yet another new twist to this emerging field (8–13). Chirality is inherently a three-dimensional (3D) phenomenon and occurs, for example, for DNA, cholesteric liquid crystals, screws, and circular metal helices (14). Chiral optical materials mix electrical and magnetic responses such that magnetic dipoles are excited by the electric component of the light field and vice versa. For pure chirality, the locally induced magnetic (electric) dipoles need to be parallel to the local exciting electric (magnetic) field. In this case, the eigenpolarizations correspond to circular polarization of light, whereas they are elliptic in the more general non-parallel (i.e., bianisotropic) case (15, 16). For example, chiral metallic metamaterial structures have led to giant gyrotropy (9), circular dichroism (10), and negative phase velocities (8) at microwave (11) and far-infrared frequencies (12). However, all these phenomena have been restricted to narrow frequency ranges, which is a major drawback for many potential applications.

In metamaterials, the narrow frequency response originates from the internal resonances of the individual building blocks. In ideal effective media, the interaction among these building blocks is negligible. The situation is reversed in, for example, cholesteric liquid crystals where the building block (the motif) exhibits only a negligible resonance. There, the interaction among the periodically arranged unit cells is crucial. It leads to Bragg resonances that are again fairly narrow. In our work on gold-helix structures, we combine internal and Bragg resonances leading to a broadband response. Strictly speaking, these metamaterial structures lie in between photonic crystals and 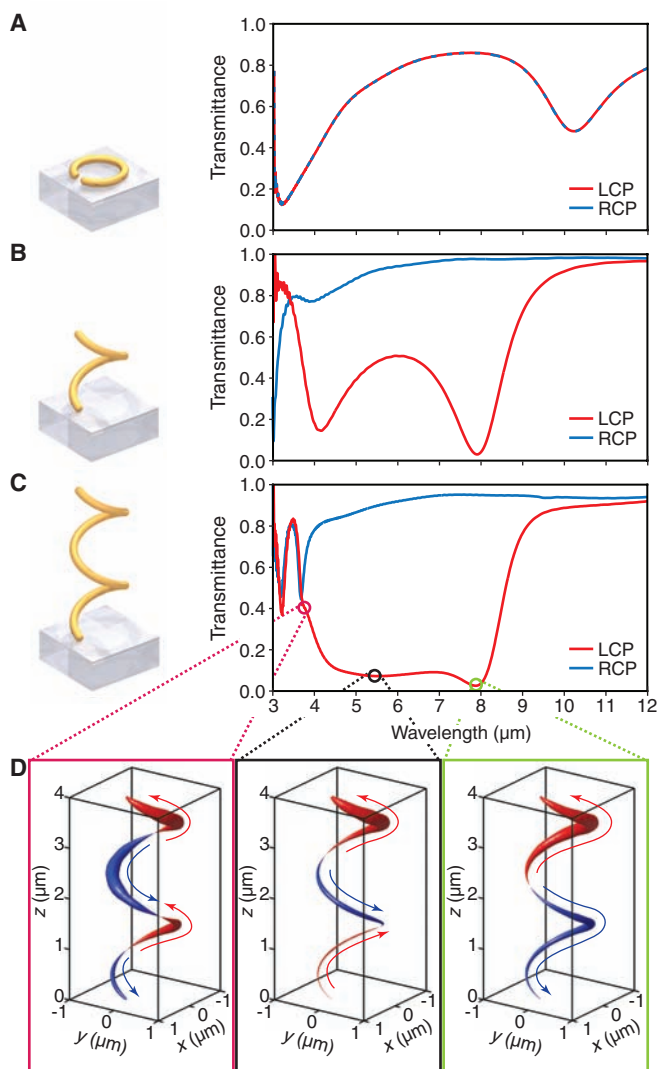effective media; hence, we refrained from retrieving effective material parameters in this work [in contrast to recent theoretical work (17)].

The geometry and the anticipated optical response are illustrated in Fig. 1 [for computational details, see (18)]. We start with a usual split-ring resonator (SRR) (Fig. 1A), a ring with a slit that can be viewed as a tiny resonant electromagnet (19–21) into which the incident light field induces a circulating and oscillating electric current, giving rise to a local magnetic field (magnetic dipole). Adiabatically pulling one end of this planar SRR out of the plane leads to one pitch of a circular helix (Fig. 1B). Thus, the electromagnetic modes of SRRs and helices with one pitch are closely related. Intuitively, a helix under normal incidence of light acts somewhat similarly to an SRR under oblique incidence with respect to the direction normal to the SRR plane. However, extrinsic chirality (22, 23) observed for planar arrays of SRRs excited under oblique incidence (24) also leads to additional linear birefringence (22, 24). Hence, in general, the polarization eigenstates do not correspond to circular



**Fig. 1.** Connection between split-ring resonators (SRRs) and metal helices. The 2 by 2 μm unit cells with 2 μm helix pitch used in the calculations in (A) to (C) are shown in the left column, normal incidence transmittance spectra for light impinging from the air side (no analyzer behind sample) in the right column. RCP and LCP refer to right and left-handed circular polarization of the incident light, respectively. (**A**) Planar SRR. Here, the RCP and LCP spectra are indistinguishable. (**B**) Adiabatically pulling the metal wire of an SRR out of the substrate plane leads to one pitch of a (left-handed) metal helix. (**C**) Two helix pitches (left-handed). (**D**) Snapshots of the electric current distribution along the metal wire for the three wavelengths [open dots in (C)]. The absolute value of the current is encoded by the curve thickness, the sign by red and blue (see arrows).

[1]Institut für Angewandte Physik and DFG-Center for Functional Nanostructures (CFN), Universität Karlsruhe (TH), Wolfgang-Gaede-Straße 1, D-76131 Karlsruhe, Germany. [2]Institut für Mikrostrukturtechnik, Forschungszentrum Karlsruhe in der Helmholtz-Gemeinschaft, D-76021 Karlsruhe, Germany. [3]Institut für Nanotechnologie, Forschungszentrum Karlsruhe in der Helmholtz-Gemeinschaft, D-76021 Karlsruhe, Germany.

*To whom correspondence should be addressed. E-mail: Justyna.Gansel@physik.uni-karlsruhe.de

but rather to elliptic polarization in that case. Linear birefringence is largely eliminated in our 3D helix design. Indeed, for the conditions of Fig. 1B, intensity conversion of the incident right-handed circular polarization (RCP) with high transmittance is below 5% in the 3.75 to 7.5 μm range.

The situation gets more complex for the case of two helix pitches (Fig. 1C). Intensity conversion of incident circular polarization is again low (below 5% in the same sense as above). However, we find a transition from sharp resonances for one helix pitch and left-handed circular polarization (LCP) in Fig. 1B to a broad stop band for two pitches in Fig. 1C (LCP). To clarify the nature of this broad stop band, we depict snapshots of the current distribution for three selected characteristic wavelengths (Fig. 1D). The three depicted modes closely resemble standing waves; that is, the positions of their current nodes change only slightly with time. The number of nodes decreases from three to one as wavelength increases for the three modes. The superposition of these three modes leads to the broad spectral response. This behavior is somewhat analogous to that for coupled SRRs (16), where magnetization waves (25) can form bands out of previously sharp individual resonances. In other words, in addition to the internal resonances, the Bragg resonance becomes important as well. The calculations are rather similar if we treat the metal as an ideal conductor rather than as a Drude free-electron metal with finite plasma frequency and damping. This observation indicates that the effects can, in principle, be scaled by structure size to any desired wavelength range, provided that the operation wavelength is sufficiently below the metal plasma frequency. This observation also indicates that, in an ideal structure, the missing light for the low-transmittance circular polarization is reflected rather than absorbed.

Our fabrication of corresponding structures for mid-infrared frequencies is outlined in Fig. 2. The idea is to infill a polymer template by electrochemical deposition of a metal [for experimental details, see (18)]. We chose gold because of its excellent optical properties at mid-infrared wavelengths and because, unlike silver, it does not deteriorate with time. Helix-shape air voids in the polymer structure are required for this purpose. Most previous work on direct laser writing (DLW) of 3D polymer structures has used negative-tone photoresists (26); the work reported in (27) is a notable exception. For negative-tone photoresists, only the sufficiently exposed regions remain after the development process. However, because of the proximity effect, fabrication of narrow pores in a bulk matrix is rather difficult in this case. Thus, we used a positive-tone resist for which only those regions that are sufficiently exposed by light are removed in the development process. Figure 3 shows corresponding structures made by using a commercially available 3D DLW system. To allow for electrochemical dep-

osition, a 25-nm thin optically transparent film of indium-tin oxide (ITO) is evaporated as the cathode onto a glass substrate before the photoresist is spun on. Typically, we use a photoresist thickness of 10 μm. After development, the structure is placed into an electrochemical cell, where a voltage is applied between the ITO film (at one side of the glass substrate) and the anode, which is immersed in the electrolyte. A constant current source controls the electrical current and, hence, the growth rate. After gold infiltration up to a certain level determined by the current density
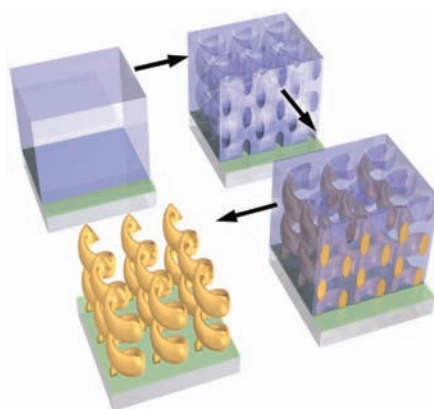
**Fig. 2.** A positive-tone photoresist (blue) is spun onto a glass substrate covered with a 25-nm thin film of conductive indium-tin oxide (ITO) shown in green. After 3D DLW and development, an array of air helices in a block of polymer results. After plating with gold in an electrolyte, the polymer is removed by plasma etching, leading to a square array of free-standing 3D gold helices.

**Fig. 4.** Normal-incidence measured and calculated transmittance spectra (no analyzer behind sample) are shown in the left and right columns. LCP and RCP are depicted in red and blue, respectively. (**A**) Slightly less than one pitch of left-handed helices, (**B**) two pitches of left-handed helices, and (**C**) two pitches of right-handed helices (see insets). For wavelengths longer than 6.5 μm, the glass substrate in the experiments becomes totally opaque. Hence, transmittance cannot be measured. For wavelengths below 3 μm, light can be diffracted into the glass substrate ($a = 2$ μm and refractive index $n = 1.5$), giving rise to Wood anomalies.

and the growth time, we completely remove the polymer by exposing the composite structure to air plasma. Oblique-view electron micrographs of the gold structures fabricated (Fig. 3B) show that these structures have a fairly small gold sur-
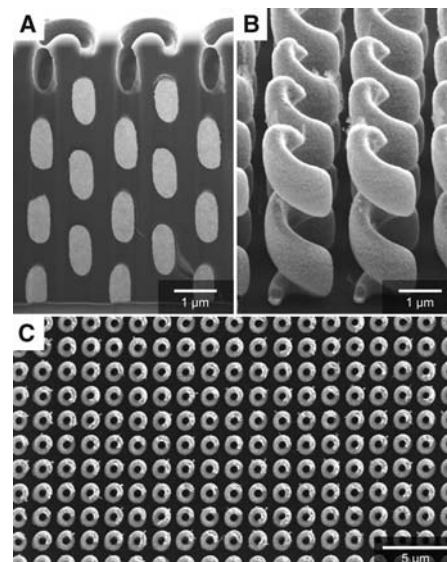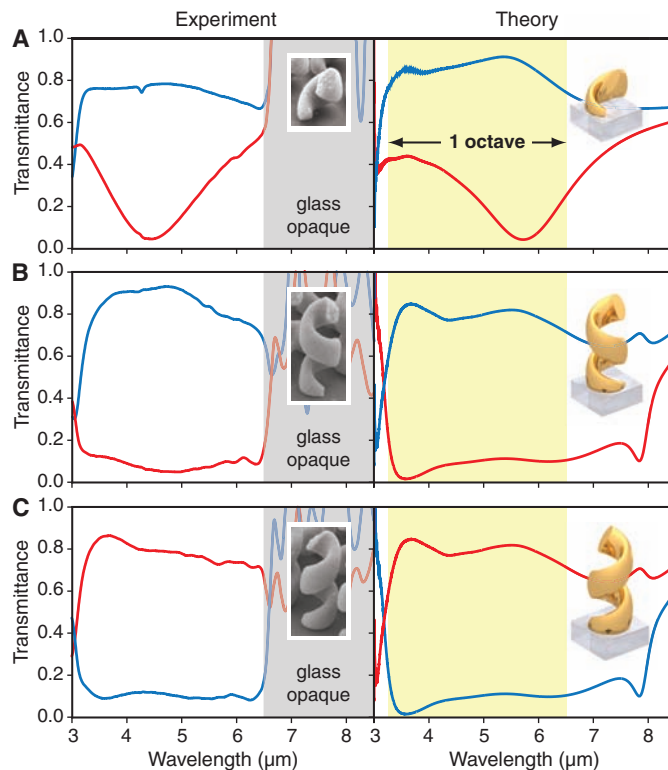
**Fig. 3.** (**A**) Focused-ion-beam (FIB) cut of a polymer structure partially filled with gold by electroplating (compare lower right part of Fig. 2). (**B**) Oblique view of a left-handed helix structure after removal of the polymer by plasma etching. (**C**) Top-view image revealing the circular cross section of the helices and the homogeneity on a larger scale. The lattice constant of the square lattice is $a = 2$ μm.

face roughness and come close to the ones theoretically anticipated in Fig. 1. Their footprint is 40 by 40 µm.

Figure 4 compares measured and calculated optical transmittance spectra for circular polarization of the incoming light propagating along the helix axis. Broadband optical spectroscopy in the few-µm wavelength range using incident circular polarization of light is not standard at all. Thus, by introducing the combination of a linear polarizer and a mid-infrared super-achromatic quarter-wave plate, we have specifically modified a commercial Fourier-transform spectrometer combined with a microscope for that purpose (18). The measured spectra in Fig. 4 reveal the theoretically anticipated blocking of one of the two circular polarizations, whereas the other circular polarization is transmitted. A large transmittance ratio results in the wavelength range from 3.5 to 7.5 µm, which exceeds one octave. Some engineering of the helix parameters would allow for further improvement of the suppression ratio. For conical helices with a diameter that continuously increases along the helix axis—rather than for the constant helix diameter discussed here—antenna theory (28, 29) promises bandwidths considerably exceeding one octave. This approach could lead to a further increase of the circular-polarizer operation bandwidth.

Metallic wire-grid linear polarizers ("one-dimensional metamaterials") have been known since the pioneering experiments on electromagnetic waves by Heinrich Hertz in 1887. Nowadays, they are still widely used for broadband applications. Because of the obvious wavelength dependence of quarter-wave plates, broadband conversion of linear into circular polarization is nontrivial in many frequency ranges. Our 3D metamaterial based on metal helices can be viewed as the circular analog of Hertz's device.

### References and Notes

1. D. R. Smith, J. B. Pendry, M. C. K. Wiltshire, *Science* **305**, 788 (2004).
2. C. M. Soukoulis, S. Linden, M. Wegener, *Science* **315**, 47 (2007).
3. V. M. Shalaev, *Nat. Photon.* **1**, 41 (2006).
4. J. B. Pendry, *Phys. Rev. Lett.* **85**, 3966 (2000).
5. U. Leonhardt, *Science* **312**, 1777 (2006).
6. J. B. Pendry, D. Schurig, D. R. Smith, *Science* **312**, 1780 (2006).
7. D. Schurig *et al.*, *Science* **314**, 977 (2006).
8. J. B. Pendry, *Science* **306**, 1353 (2004).
9. A. V. Rogacheva, V. A. Fedotov, A. S. Schwanecke, N. I. Zheludev, *Phys. Rev. Lett.* **97**, 177401 (2006).
10. M. Decker, M. W. Klein, M. Wegener, S. Linden, *Opt. Lett.* **32**, 856 (2007).
11. E. Plum *et al.*, *Phys. Rev. B* **79**, 035407 (2009).
12. S. Zhang *et al.*, *Phys. Rev. Lett.* **102**, 023901 (2009).
13. M. Wegener, S. Linden, *Physics* **2**, 3 (2009).
14. E. Hecht, *Optics* (Addison-Wesley, San Francisco, ed. 4, 2002), chap. 8.
15. M. S. Rill *et al.*, *Nat. Mater.* **7**, 543 (2008).
16. N. Liu, H. Liu, S. Zhu, H. Giessen, *Nat. Photon.* **3**, 157 (2009).
17. M. G. Silveirinha, *IEEE Trans. Antenn. Propag.* **56**, 390 (2008).
18. Materials and methods are available as supporting material on *Science* Online.
19. J. B. Pendry, A. J. Holden, D. J. Robbins, W. J. Steward, *IEEE Trans. Microw. Theory Tech.* **47**, 2075 (1999).
20. S. Linden *et al.*, *Science* **306**, 1351 (2004).
21. R. Abdeddaïm, G. Guida, A. Priou, B. Gallas, J. Rivory, *Appl. Phys. Lett.* **94**, 081907 (2009).
22. E. Plum, V. A. Fedotov, N. I. Zheludev, *Appl. Phys. Lett.* **93**, 191911 (2008).
23. E. Plum *et al.*, *Phys. Rev. Lett.* **102**, 113902 (2009).
24. C. Enkrich *et al.*, *Phys. Rev. Lett.* **95**, 203901 (2005).
25. E. Shamonina, L. Solymar, *J. Magn. Magn. Mater.* **300**, 38 (2006).
26. K. Busch *et al.*, *Phys. Rep.* **444**, 101 (2007).
27. W. Zhou *et al.*, *Science* **296**, 1106 (2002).
28. J. S. Chatterjee, *J. Appl. Phys.* **24**, 550 (1953).
29. J. D. Dyson, *IRE Trans. Antennas Propag.* **7**, 181 (1959).
30. We thank I. Staude for help regarding the optical measurements and C. E. Kriegler for discussions. We acknowledge support by the Deutsche Forschungsgemeinschaft (DFG) and the State of Baden-Württemberg through the DFG Center for Functional Nanostructures (CFN) within subprojects A1.4 and A1.5. The project PHOME acknowledges the financial support of the Future and Emerging Technologies (FET) program within the Seventh Framework Programme for Research of the European Commission, under FET Open grant 213390. The project METAMAT is supported by the Bundesministerium für Bildung und Forschung (BMBF). The research of S.L. is further supported through a Helmholtz-Hochschul-Nachwuchsgruppe (VH-NG-232) and that of G.v.F. through a DFG Emmy-Noether fellowship (DFG-Fr 1671/4-3). The Ph.D. education of J.K.G., M.T., M.S.R., and M.D. is embedded in the Karlsruhe School of Optics and Photonics (KSOP).

# Control of Spin Precession in a Spin-Injected Field Effect Transistor

Hyun Cheol Koo,[1] Jae Hyun Kwon,[1] Jonghwa Eom,[1,2] Joonyeon Chang,[1]* Suk Hee Han,[1] Mark Johnson[3]

Spintronics increases the functionality of information processing while seeking to overcome some of the limitations of conventional electronics. The spin-injected field effect transistor, a lateral semiconducting channel with two ferromagnetic electrodes, lies at the foundation of spintronics research. We demonstrated a spin-injected field effect transistor in a high-mobility InAs heterostructure with empirically calibrated electrical injection and detection of ballistic spin-polarized electrons. We observed and fit to theory an oscillatory channel conductance as a function of monotonically increasing gate voltage.

**M**any types of spintronic devices have been proposed, investigated, and developed. However, the spin-injected field effect transistor (spin FET), which lies at the heart of spintronics, has yet to be realized.

Proposed by Datta and Das (1), the demonstration of a spin FET involves spin injection and detection using a ferromagnetic source and drain. However, a special feature of the spin FET is the periodic modulation of source-drain conductance as controlled by gate voltage–induced precession of the injected spins. Electrical spin injection and detection have been demonstrated in a variety of semiconductors (2–6). Carrier spin precession has been induced by using an external magnetic field and detecting the Hanle effect, a Lorentzian-shaped magnetoresistance caused by precessional dephasing of diffusing spins, in materials with relatively small spin-orbit interaction such as GaAs and Si (3–5). However, modulating the channel conductance by using an electric field to induce spin precession has remained elusive. A material with large spin-orbit interaction will not permit the observation of the Hanle effect, yet this type of material is necessary for gate voltage–induced spin precession. These two phenomena are mutually exclusive within any single material. We used a high-mobility InAs heterostructure with strong intrinsic spin-orbit interaction α, and we measured the nonlocal channel conductance (5, 6) rather than the direct source-drain conductance suggested by Datta and Das. Conventional lateral spin valve techniques measured the population of ballistic spins. Shubnikov–de Haas (SdH) experiments provided an independent measurement of the dependence of the spin-orbit interaction on gate voltage. Apart from a small phase shift, the oscillatory conductance that we measured fits to theory (1) with no adjustable parameters. The temperature dependence indicates that the modulation is only observed when the injected electrons have ballistic trajectories to the detector.

A conventional lateral spin valve device (Fig. 1A) is a convenient structure to investigate spin injection and detection for several reasons. First, the ferromagnetic (FM) electrodes have a uniaxial shape anisotropy that can create binary

[1]Center for Spintronics Research, Korea Institute of Science and Technology (KIST), 39-1 Hawolgok-dong, Seongbuk-gu, Seoul, 136-791, Korea. [2]Department of Physics, Sejong University, 98 Gunja-dong, Gwangjin-gu, Seoul, 143-747, Korea. [3]Naval Research Laboratory, 4555 Overlook Avenue SW, Washington, DC 20375, USA.

*To whom correspondence should be addressed. E-mail: presto@kist.re.kr